Printed ISSN 1330–0008
Online ISSN 1333–9125
CD ISSN 1333–8390
CODEN FIZAE4

SOME CHARACTERISTIC PHYSICAL PROPERTIES OF NICKEL OXIDE POWDER

S. A. GAD[a], M. BOSHTA[a], A. M. ABO EL-SOUD[a] and M. Z. MOSTAFA[b]

[a]*Solid State Physics Department, National Research Center, El-Boohoos str., 12311 Dokki, Giza, Egypt*

[b]*Ceramic, Refractories and Building Materials Department, National Research Center, El-Bohoos st., 11312 Dokki, Giza, Egypt*

Received 27 October 2008; Revised manuscript received 15 April 2009
Accepted 18 November 2009 Online 31 December 2009

Nickel oxide powder was prepared by firing spec pure $NiCO_3$ in air for 6 hours at different firing temperatures ranged from 800°C to 1200°C. The crystal structure of all samples is a cubic structural as obtained from XRD study. The diffuse reflectance of different samples of NiO was measured at room temperature in the wavelength range from 200 to 2000 nm. The energy gap of NiO samples was then deduced as well as the position and number of different transitions which were found to be dependent on the firing temperature. The electrical conductivity σ_m was measured over temperature range from 50°C to 320°C and frequency range from 42 Hz to 5 MHz. The conductivity decreases with increasing firing temperature and increases with frequency. The activation energy was calculated and was found to increase with increasing firing temperature. Electron spin resonance (ESR) spectra were recorded at room temperature as first derivatives using an X-band spectrometer with a magnetic field modulation of 100 kHz. The intensity of the ESR-spectra of NiO samples decreases with increasing firing temperature.

PACS numbers: 77.84.Bw, 81.05.Je, 72.80.Jc UDC 538.911, 538.93, 537.312

Keywords: nickel oxide powder, crystal structure, energy gap, electrical conductivity, electron spin resonance spectra

1. Introduction

The transition metal oxides form a group of predominantly ionic solids which exhibit a wide range of optical and electrical properties. They are now being widely used in chemistry and electronics, as well as in magnetic devices, in heterogeneous catalysis and in a number of other applications. Nickel oxides have a wide range of application due to their excellent chemical stability as well as their optical and magnetic properties. They have been used as antiferromagnetic materials in form of thin films [1], for electrochromic display devices thin film [2], p-type transport conducting films [3] and functional layer materials for chemical sensors [4].

Nickel oxide is one of the transition metal oxides which have attracted a considerable interest because it should be a conductor according to simple energy band theory, but experimentally is found to be an insulator in its pure stoichiometric form. This behavior has been discussed by different authors; Verwey and DeBoer [5] and Mott [6] suggested that for NiO the Heitler-London approach might lead to a better approximation. In this case the presence of nickel ions of different valences would be a necessary condition for the electrical transport.

It has been found that nickel oxide is mostly a metal defect p-type semiconductor ($Ni_{1-x}O$). The predominant defects being cation vacancies and electronic holes. However, the nonstoichiometry, x, in this oxide is very low. Thus the determination of nonstoichiometry as a function of temperature and oxygen pressure is very difficult and consequently the results obtained by various authors differ considerably [7]. The aim of the present work is to clarify the situation by studying the electrical, optical and ESR spectra of nonstoichiometric NiO prepared from nickel carbonate as a function of the firing temperatures in air.

2. Experimental

It is well known that NiO can be prepared either by firing Ni metal or one of its salts in oxygen or air atmosphere. So, in this work, NiO was prepared by firing spec pure $NiCO_3$ in air for 6 hours at different firing temperatures, ranged from 800°C to 1200°C.

The reaction was followed by differential thermal analysis (DTA) which showed that all firing temperatures above 600°C gave a complete transformation of $NiCO_3$ to NiO, while below this temperature some traces of carbonates still exist. X-ray diffraction (XRD) patterns of the prepared samples were recorded with a Diano X-ray diffractometer using monochromatized Cu Kα radiation of wavelength $\lambda = 1.54$ Å from a fixed source operated at 45 kV and 9 mA.

Diffuse reflectance measurements were done in the wavelength range from 200 to 2000 nm using Jasco (V-570) spectrophotometer. Electron spin resonance was recorded as first deriation using an X-band spectrum with a magnetic field modulation of 100 kHz using Bruker Elexsys 500, receiver gain 60, sweep width 6000 center at 4389 Ø, with a nominal microwave power 0.20 Watt. The prepared samples were ground carefully and compressed at two tons on disc of diameter 1.5 cm for electrical measurements. The ac conductivity was measured using a computerized RLC circuit type (Hioki 3532 50 LCR Hi-Tester; Japan) with frequency range 42 Hz − 5 MHz and over the temperatures range from 50°C to 320°C.

3. Results and discussion

The produced fired samples have been studied by X-ray diffraction technique, which revealed that the predominantly obtained phase is nickel oxide with the cubic structure in the firing temperatures range between 800°C and 1200°C, as shown in Fig. 1. The XRD peak intensity has slightly increased with firing temperatures without any change in peak positions. The peaks width β (after correction for instrumental broadening) was used to determine the average particle size G and the strain η using the following relation [8]

$$\beta \cos\theta = \frac{0.89\lambda}{G} + \eta \sin\theta \,. \tag{1}$$

Particle sizes G were determined from the above equation, where θ is the diffraction for a particular Bragg diffraction peak, and β is the (corrected) full width (in radians) of the peak at half maximum (FWHM) intensity. The correction to the measured FWHM β_s for a sample peak was made to accommodate systemic instrumental broadening and utilized peak widths β_q measured from a diffraction scan, taken under identical conditions, from a strain-free powdered quartz sample, with particle size ranging between 5 and 10 μm. The corrected sample peak widths were calculated as $\beta = (\beta_s^2 - \beta_q^2)^{1/2}$. Micro-strain and crystallite size contributions to β were separated using the Win-Fit program, using standard samples for estimation of instrumental broadening. The final sample particle sizes G were obtained by Fourier analysis, using the corrected profile. The diffraction peak used is the most intense diffraction one, assigned to the (200) reflection from the cubic phase, that appears at $2\theta = 43.3°$.

The plot of $\beta \cos\theta$ versus $\sin\theta$, using different Bragg lines, yields $G = 12.4$ nm as an average value for all samples and a negligible $\eta = 2.23\ 10^{-3}$. This analysis shows that the NiO samples are essentially strain-free.

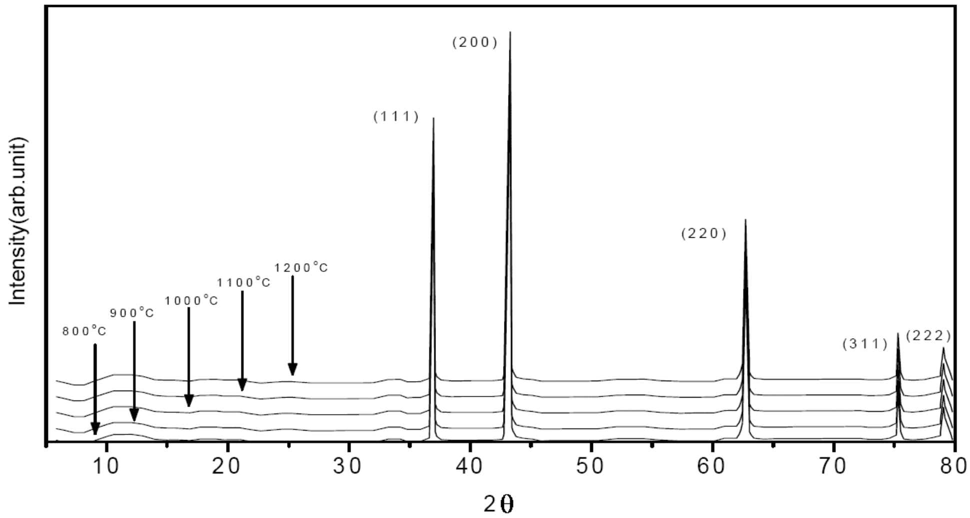

Fig. 1. XRD patterns of NiO *samples obtained at different firing temperatures.*

3.1. Optical properties

The diffuse reflectance (R) was measured as a function of wavelength from 200 to 2000 nm. The spectra within the entire frequency range are shown in Fig. 2. The energy band gap E_g can be determined from the onset of the linear increase in the diffuse reflectance as a function of firing temperatures [9]. The obtained values of E_g are shown in Table 1.

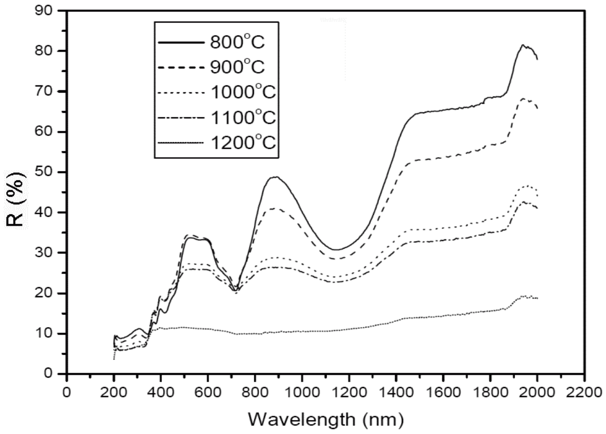

Fig. 2. The diffuse reflectance (R) versus the wavelength λ for NiO *samples obtained at different firing temperatures.*

TABLE 1. Band gap energies of NiO *obtained at different firing temperatures.*

Firing temp. (°C)	E_{g_1} (eV)	E_{g_2} (eV)	E_{g_3} (eV)	Oxide color
800	2.818	1.908	1.138	Grey
900	3.0244	2.0	1.216	Greenish grey
1000	3.5429	2.3846	1.4419	Light green
1100	3.875	2.7556	1.512	Light green
1200	4.133			Green

For the NiO samples obtained below 1200°C, three bands have been observed, with band gaps E_{g_1}, E_{g_2} and E_{g_3}, where E_{g_1} represents the fundamental energy band gap, E_{g_2} represents the energy band gap due to the crystal field and E_{g_3} represents the energy band gap due to the transition from 2p-states to 3d-states.

For the NiO sample obtained at 1200°C, only one band was observed. In the decomposition process of $NiCO_3$ by raising the firing temperature, Ni^{+3} may refer to a structure that contains Ni^{+2} ions with holes, as an effect of the presence of the localized traces of CO_2 in the lattice and not to the existing of Ni_2O_3 in the prepared non-stoichiometric NiO samples. So Ni^{+3}/Ni^{+2} ratios would decrease with increasing the firing temperature, suggesting interstitial oxygen atoms in the structure. By increasing the firing temperature, the oxygen-rich content diffuses out, and so reducing the chemical valency of Ni to get the nonstoichiometric NiO with the valency of Ni moves to be Ni^{+2} accompanied by the formation of hole carriers. In order to describe the nature of the energy gap in NiO structure, two facts have to be taken into consideration. First, the overlap between the two d-functions, even though it is small. Second, the state of the crystal field effect. As a consequence, each d-state possesses dispersion and the d-states are band-like rather than a succession of individual states. Owing to the knowledge of the well localized d-functions, the 3d-band can be described using the tight-binding method. As a result of that, the origin of the crystal field separation of NiO structure is attributed to the ionicity and covalency, with the covalent effects predominant. Thus, the separation due to the crystal field and d-band originates mainly from the hybridization of processes [10].

It is also possible that the 2p and 4s levels of NiO spread out in the bands. In this case, the 3d electrons remain localized about the lattice sites which can be an acceptable actual picture which seems adoptable to NiO. The 3d-band can be considered as representing the whole of the 3d states. These can be associated with a broadening to each final d level, giving rise to a broad density of states. On the other hand, the electronic charge-density maps of NiO justify a perfect ionic crystal, permitting crystal-field-effect explanation for the evaluation of the ionic and covalent contribution in NiO [10]. So at lower decomposition temperatures of nickel carbonate to get NiO, the resulting crystalline phases are characterized by non-stoichiometry, covalency-ionic bonding, presence of CO_2 traces and interstial oxygen, as well as presence of some holes. This results in obtaining three different energy gaps, one of them is the fundamental essential 3d to 4s [11], the second of the crystal field and the last may be due to transition from 2p-3d as well as the hybridization from 4s to 2p.

3.2. Electrical conductivity

The frequency dependence of the measured conductivity σ_m of the sample obtained at 1200°C at different measuring temperatures is shown in Fig. 3. The obtained results for σ_m are found to be more or less independent of frequency below 100 kHz. A similar frequency independent response at low frequency region has earlier been reported for NiO thin films [12]. This low frequency region corresponds to the dc conductivity where the inter-well hopping responsible for pure dc conduction completely dominates over the intra-well hopping associated with pure ac conduction [12−14]. At still higher frequencies, σ_m shows marked increase with frequency. A careful analysis of σ_m as the sum of $\sigma_{\rm dc}$ and $\sigma_{\rm ac}$ reveals the following general trends;

(i) At lower frequencies and higher temperatures (> 100°C), σ_m is very nearly equal to $\sigma_{\rm dc}$ since $\sigma_{\rm ac} = \sigma_m - \sigma_{\rm dc}$ is small (Fig. 3). At lower frequencies and lower temperatures, σ_m is slightly higher than $\sigma_{\rm dc}$ and the contribution due to $\sigma_{\rm ac}$ is barely distinguishable.

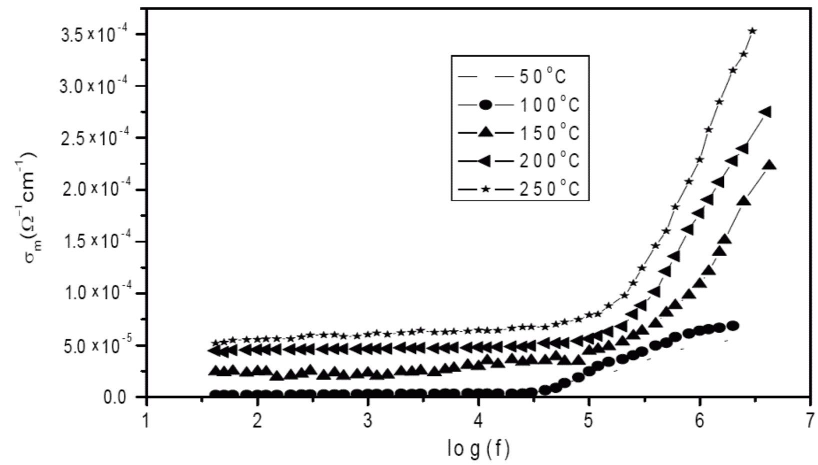

Fig. 3. The measured ac conductivity of NiO *sample obtained at firing temperature* 1200°C *versus the frequency at different measuring temperatures.*

(ii) At higher frequencies and higher temperatures, the contribution of σ_{ac} to σ_m becomes larger, though the contribution of σ_{dc} cannot be neglected. At higher frequencies and lower temperatures, σ_{ac} contribution to σ_m completely predominates over that due to σ_{dc}. The variation of pure ac conductivity, $\sigma_{\text{ac}} = \sigma_m - \sigma_{\text{dc}}$ with frequency of the applied signal for one of the tested samples (as an example) is shown in Fig. 4. At low frequencies, the probability for inter-well hopping predominates over that due to intra-well hopping and $\sigma_m \sim \sigma_{\text{ac}}$ [13, 14]. The probability for

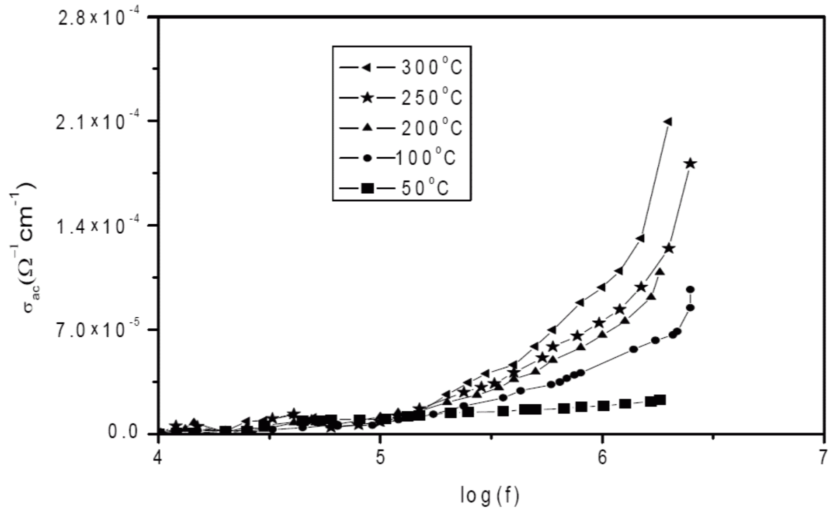

Fig. 4. Pure ac conductivity of NiO *sample fired at* 1200°C *versus the frequency at different measuring temperatures.*

inter-well charge transfer by hopping over the barrier (HOB) and hopping through the barrier (HTB) are given by [15]

$$W = W_0 \exp(E_0/kT)\,, \tag{2}$$

where E_0 is the activation energy for hopping, k the Boltzmann constant and T the absolute temperature. The frequency factor, W_0, is given by

$$\begin{aligned} W_0 &= \left(\pi/(4kT)E_0\right)^{1/2} J^2 h/(2\pi), && \text{for hopping through the barrier} \\ &= \omega_0/(2\pi), && \text{for hopping over the barrier} \end{aligned}$$

where J is the matrix element of the perturbing potential between the whole wave-functions centered at neighboring Ni^{2+} ions, h is the Planck's constant and ω_0 is the longitudinal optical phonon frequency [15]. From Eq. (2), it is clear that the probability for both HOB and HTB increase as temperature is increased. Thus at higher temperatures and lower frequencies σ_m is dominated by inter-well hopping and $\sigma_{\rm ac}$ does not contribute to σ_m. However, as the signal frequency is increased to higher values, there is a high probability of occurrence of intra-well hopping by which $\sigma_{\rm ac}$ contributes to σ_m [13, 14]. At lower temperatures (50°C and 100°C), the probability of occurrence of the inter-well charge transfer decreases according to Eq. (2) and even at low frequencies $\sigma_{\rm ac}$ contributes markedly to σ_m. At these lower temperatures, as the frequency of the applied signal is increased, the probability of occurrence of the intra-well hopping completely dominates over $\sigma_{\rm dc}$ (Figs. 3 and 4). However, even at room temperature and in the MHz frequency range, $\sigma_{\rm dc}$ contributes markedly to σ_m which may be attributed to the percolation of the potential wells associated with Ni^{2+} vacancies [13, 14]. This is justifiable owing to the very high density of Ni^{2+} vacancies concentrated at the highly disordered and defective grain boundaries of the NiO nanoparticles [1 − 18].

The ac conductivity was measured over the range of temperatures from 50°C to 320°C. The temperature dependence of the ac conductivity for different NiO samples is shown in Fig. 5. It is clear from this figure that the conductivity increases with increasing temperature for all samples. At high temperatures, the ac conductivity shows a flat maximum followed by a decrease. The reason for such a decrease may lie in the temperature dependence of one or both the mobility and the carrier concentration [19].

The activation energy calculated from the dependence of conductivity on the temperature is shown in Fig. 6 for NiO samples prepared at different firing temperatures. From this figure, it is clear that the activation energy increases when increasing the preparation firing temperature. This increase in activation energy may be due to the increase of the oxygen concentration in the samples. The activation energy is supposed to be due in part or entirely to the ionization of the shallow nickel vacancy-acceptor level [20]. Mrowec and Grzeik [7] found from the pressure dependence of oxidation rate of nickel and for the nonstoichiometry of nickel oxide that the predominant defects are doubly-ionized cation vacancies and electronic holes.

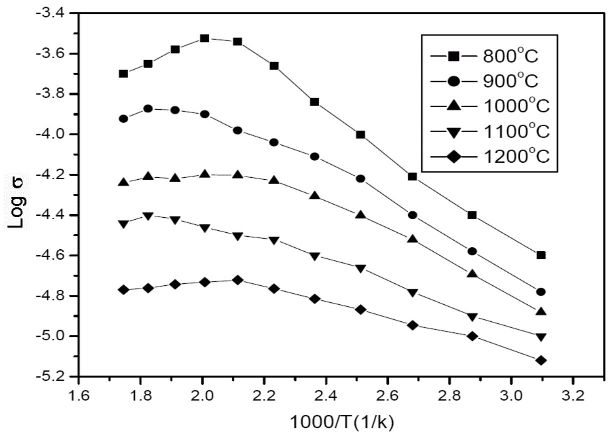

Fig. 5. Conductivity of the NiO *samples prepared at different firing temperatures versus* 1000/K.

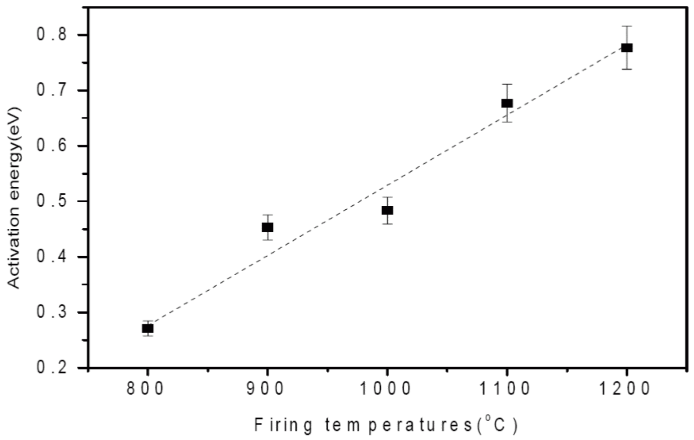

Fig. 6. Activation energy versus the firing temperature for the NiO *samples.*

3.3. ESR Measurements

Electron spin resonance (ESR) spectra were recorded as first derivatives using an X-band spectrometer with a magnetic field modulation of 100 KHz. The measurements were carried out at room temperature. The modulation amplitude was far below the level assumed to distort the line shape. Figure 7 shows the ESR spectra recorded at 300 K. It is clear from this figure that the spectra exhibit only one broad resonance line, the line width and peak to peak position, however, increase with increasing firing temperature. From this figure it can also be seen that the intensity of the spectra increases with increasing firing temperature from 800°C

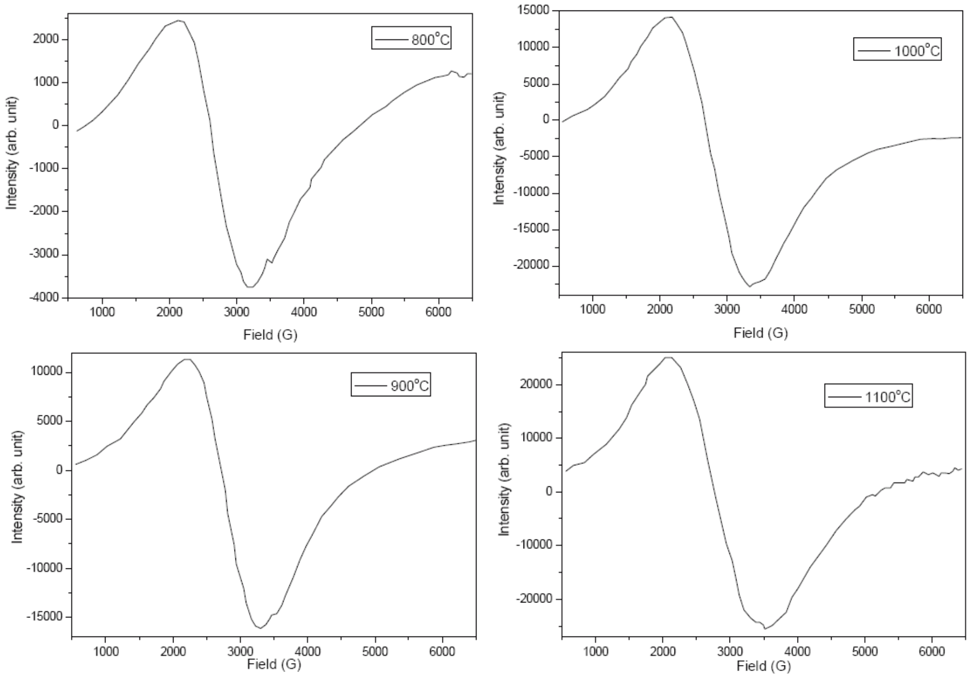

Fig. 7. ESR spectra of NiO *prepared at different firing temperatures.*

to 1100°C. Correspondingly, the obtained g-values for the prepared NiO samples having an ESR spectral response were mainly $g_1 = 1.98$ and $g_2 = 2.2$. At firing temperatures higher than 1100°C, i.e. at 1200°C, a very poor spectral response for ESR was obtained. This means that the sample prepared at this temperature reached a more stoichiometric one. This result may be explained on the bases that the NiO prepared at different firing temperatures in air up to 1100°C has a mixed valency of Ni^{+2} and Ni^{+3} with different ratios. Gendron et al. [21] remark that the line-width increases with the degree of nickel substitution in $LiCO_{1-y}Ni_yO_2$ and that the Ni^{+3} ($3d^7$) ions located in octahedral crystallographic sites, with a low spin state, i.e. 1/2, give the corresponding ESR transition due to the localized g magnetic

TABLE 2. The g values of NiO *samples as a function of the preparation firing temperatures.*

Firing temperature (°C)	g_1	g_2
1100	1.98	2.09
1000	1.89	2.1
900	1.98	2.1
800	1.98	2.2

factor $g \simeq 2.12$. Moreover, Kawabala [22] demonstrated that the broadening of ESR signal of fine metal particle suffers from quantum size effect and can be correlated to the size of the particles. Table 2 shows the g values of samples for different preparation firing temperatures which represent the presence of Ni^{+3} and Ni^{+2} together.

4. *Conclusion*

Nickel oxide prepared by firing spec pure $NiCO_3$ in air has a nonstoichiometric structure at firing temperatures below 1200°C, whereas that prepared at 1200°C is more stoichiometric. All samples prepared at firing temperatures from 800°C to 1200°C have only NiO phase with cubic structure.

The optical energy gap was calculated from the diffuse reflectance. It shows that there are three energy band gaps for all samples prepared below 1200°C, while the sample prepared by firing at 1200°C has only one fundamental energy gap of 4.133 eV. The fundamental energy band gap varied from 2.818 eV to 4.133 eV by changing the preparation firing temperature from 800°C to 1200°C. The crystal field effect energy gap (E_{g_2}) varied from 1.908 eV to 2.755 eV with firing temperature from 800°C to 1100°C, while E_{g_3} varied from 1.138 eV to 1.512 eV within the same temperature range. The ac conductivity of NiO samples has the same trend like the dc conductivity at lower frequency and lower measuring temperature, i.e. it is frequency independent. But at high frequency and high measuring temperature, the ac conductivity is more dependent on the frequency and increases when increasing both frequency and measuring temperature. The activation energy of prepared NiO samples increases with increasing the firing temperature used in preparation from 0.271 eV to 0.777 eV.

The ESR spectra show only one broad resonance line, of different line width, which increases for increasing the preparing firing temperature. In addition, the intensity of the spectra increases with increasing firing temperature up to 1100°C.

References

[1] E. Fujii, A. Tomozawa, H. Torii and R. Takayama, Jpn. J. Appl. Phys. **35** , 2 (1996) L328.

[2] W. Gouda and K. Shiiki, J. Mag. Mater. **205** (1999) 136.

[3] H. Sato, T. Minam, S.Takata and T. Yamad, Thin Solid Films **23** (1993) 3001.

[4] H. Kumagai, M. Matsumoto, K. Toyoda and M. Obara, J. Mater. Sci. Lett. **15** (1996) 1081.

[5] J. H. Deboer and F. Verwey, J. Proc. Phys. Soc. **49** (1937) 59.

[6] N. F. Mott, Proc. Phys. Soc. A **62** (1949) 416.

[7] S. Mrewec and Z. Grzesik, J. Phys. Chem. Solids **65** (2004) 1654.

[8] P. Dutta, A. Manivannan and M. S. Seehra, Phys. Rev. **70** (2004) 174428.

[9] A. M. Abo El-Soud, F. El-Akkad, S. Hammad and N. A. Ali, J. Mater. Sci., Material in Electronics **2** (1991) 171.

[10] J. Hugel and C. Carabatos, J. Phys. C; Solid State Phys. **16** (1983) 6713.

[11] D. Franta, B. Negulescu, L. Thomas, P. R. Dahoo, M. Guyot, I. Ohlidal, J. Mistrik and T. Yamaguchi, Appl. Surface Science **244** (1-4) (2005) 426.

[12] P. Lunkenheimer, A. Loidl, C. R. Ottermann and K. Bange, Phys. Rev. B. **44** (11) (1991) 5927.

[13] A. J. Bosman and H. J. Van Daal, Adv. Phys. **19** (1970) 1.

[14] M. Sayer, A. Mansingh, J. B. Webb and J. Noda, J. Phys. C.: Solid State Phys. **11** (1978) 315.

[15] J. Appel, Phys. Rev. B **141** (2) (1966) 506.

[16] V. Biju and M. Abdul Khadar, Mater. Res. Bull. **36** (1/2) (2001) 21.

[17] H. J. Wasserman and J. S. Vermaak, Surf. Sci. **22** (1970) 164.

[18] R. Birringer, Mater. Sci. Eng. A **117** (1989) 33.

[19] Jiin-Long Yang, Yi-Sheng Lai and J. S. Chen, Thin Solid Films **488** (2005) 242.

[20] J. G. Aiken and A. G. Jordan, J. Phys. Chem. Solids **29** (1968) 2153.

[21] F. Gendron, S. Castro-Garica, E. Popva, S. Ziolkiewiez, F. Soulette and C. Julien, Solid State Ionic **157** (2003) 125.

[22] A. Kawabata, J. Phys. Soc. Japan **29** (1970) 902.

NEKE ZNAČAJKE FIZIČKIH SVOJSTAVA PRAHA NIKAL OKSIDA

Prah nikal oksida smo pripremali 6-satnim prženjem $NiCO_3$ u zraku na nizu temperatura između 800°C i 1200°C. Kristalna struktura svih uzoraka je kubna kako smo utvrdili rentgenskom difrakcijom. Difuznu reflektivnost uzoraka NiO mjerili smo na sobnoj temperaturi u području valnih duljina 200 do 2000 nm. Utvrdili smo energijski procjep kao i položaj i broj niza prijelaza i ustanovili da ovise o temperaturi prženja. Mjerili smo električnu vodljivost σ_m na temperaturama 50°C do 320°C i u području frekvencija 42 Hz do 5 MHz. Vodljivost se smanjuje za veće temperature prženja a raste s frekvencijom. Izračunali smo aktivacijsku energiju i našli da raste s povećanjem temperature prženja. Mjerili smo spektre elektronske spinske rezonancije (ESR) na sobnoj temperaturi kao prve derivacije pomoću spektrometra u pojasu X, modulirajući magnetsko polje sa 100 kHz. Intenzitet spektara ESR uzoraka NiO smanjuje se s povećanjem temperature prženja.